VIII International Conference on Fracture Mechanics of Concrete and Concrete Structures
FraMCoS-8
J.G.M. Van Mier, G. Ruiz, C. Andrade, R.C. Yu and X.X. Zhang (Eds)

MODELING OF CORROSION-INDUCED CONCRETE DAMAGE

ANNA EMILIE A. THYBO[*], ALEXANDER MICHEL[*] AND HENRIK STANG[*]

[*] Technical University of Denmark (DTU)
Department of Civil Engineering
Brovej, Building 118, 2800 Kgs. Lyngby, Denmark
Email: aeth@byg.dtu.dk, www.byg.dtu.dk

Key words: Non-uniform corrosion, Durability, Reinforced concrete, Concrete cover cracking.

Abstract: In the present paper a finite element model is introduced to simulate corrosion-induced damage in concrete. The model takes into account the penetration of corrosion products into the concrete as well as non-uniform formation of corrosion products around the reinforcement. To account for the non-uniform formation of corrosion products at the concrete/reinforcement interface, a deterministic approach is used. The model gives good estimates of both deformations in the concrete/reinforcement interface and crack width when compared to experimental data. Further, it is shown that non-uniform deposition of corrosion products affects both the time-to cover cracking and the crack width at the concrete surface.

1 INTRODUCTION

Infrastructure constructions represent major investments for society and consequently vast efforts are made to understand and predict the service life and associated deterioration mechanisms of infrastructure constructions. A major part of these infrastructure constructions is made of reinforced concrete. One of the most important deterioration mechanisms in reinforced concrete structures is reinforcement corrosion [1]. Corrosion-induced damages, such as concrete cracking, spalling, delamination, and cross sectional reduction of the reinforcement, may cause aesthetic damages, decrease the load bearing capacity of a structure, and in the worst case lead to fatal structural consequences, such as failure.

In particular, the formation of cracks in the concrete cover as well as cross sectional reduction of reinforcement area is affecting strength and serviceability of reinforced concrete structures. Hence, corrosion-induced cover cracking has been studied to a great extent, see e.g. [2,3], and various models such as analytical, see e.g. [4,5], empirical, see e.g. [6,7], and finite element based, see e.g. [8-11], models have been suggested over the years. In general, these models are consistent with experimental data, however, recent application of experimental techniques such as x-ray attenuation [12-14] and digital image correlation [15] have highlighted that (i) corrosion products penetrate into the concrete matrix and (ii) corrosion products form non-uniformly around the circumference of the reinforcement leading to non-uniform deformations - both topics are so far relatively uncharted. The majority of the proposed models neglect these mechanisms, which may cause misleading and unrealistic results. Therefore, the influence of penetration of corrosion products as well as non-uniform formation in the concrete/reinforcement interface should be further investigated.

In the present paper an existing finite element based model [15], which simulates the expansion of uniformly deposited corrosion products - taking into account the penetration of corrosion products into the concrete matrix - and predicting the propagation of corrosion-induced damage, is taken one step further allowing for non-uniform formation of corrosion products around the circumference of the rein-

forcement. The model is accounting for the expansion of corrosion products utilizing a thermal analogy. Non-uniform corrosion is introduced assigning a specific thermal expansion to each element in the corrosion layer. Initially, the modeling approach to account for non-uniform formation of corrosion products is tested comparing numerical results with experimental observations presented in [15].

Finally, a numerical example is given to demonstrate the influence of non-uniform corrosion on the time-to corrosion-induced cover cracking.

2 MODELING APPROACH

The proposed modeling approach is based on an existing finite element method (FEM) model [10,11,15] that simulates the formation and propagation of corrosion-induced damage in a reinforced concrete body applying a discrete cracking approach. Neither micro-cracking nor the influence of cracks on the transport properties of concrete is currently included in the model.

To simulate the formation and propagation of corrosion-induced damage, the proposed model is divided into five distinct domains; concrete, reinforcement, a corrosion layer, cracking, and debonding domain (crack opening and sliding at reinforcement surface). Crack propagation along with the different domains is illustrated in Figure 1 for two different times, t_1 and t_2. The crack initiates at or near the surface of the reinforcement and subsequently propagates towards the concrete surface as observed in [12-15]. The concrete domain is described by a semi-infinite concrete body with elastic material behavior. Zero-thickness cohesive interface elements are implemented perpendicular (simulating mode-I crack propagation in the concrete cover) and circumferential (simulating mixed-mode crack propagation) to the reinforcement allowing only for crack propagation in the implemented interface elements. However, corrosion-induced crack patterns obtained from experimental investigations (see e.g. [2,3,16]) support the assumption of a prescribed crack path.

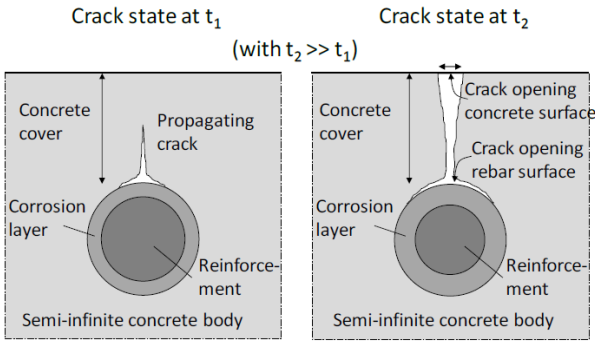

Figure 1: Crack propagation in proposed FEM model, from [10].

Cracking in the concrete cover layer is induced once tensile stresses (which are caused by the expansion of corrosion products) exceed the tensile strength of the concrete. To simulate corrosion-induced damage in the model two steps are implemented; a) calculation of the reduction of the reinforcement radius and b) calculation of the expansion of corrosion products.

Figure 2 illustrates the confined and free expansion mechanism of the corroding reinforcement assuming uniform formation of corrosion products. R_2 is the free expanding radius of the corroded reinforcement, R_1 the radius of the non-corroded part of the reinforcement and R_0 the radius of the original non-corroded reinforcement.

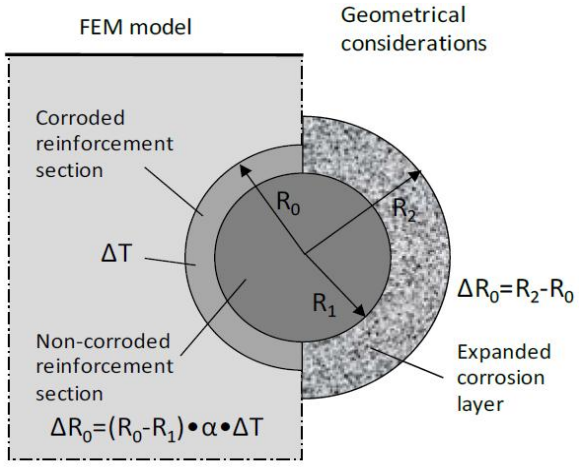

Figure 2: Load application in FEM model (left) and basic geometrical considerations of the free expansion of the corroding reinforcement (right) in crack propagation model, from [10].

From Faraday's law the reinforcement radius reduction due to corrosion i.e. the thickness of the corrosion layer is determined:

$$X(t) = R_0 - R_1 = \frac{M\, i_{corr}\, \Delta t}{z\, F\, \rho} \quad (1)$$

where M is the molar mass of the metal [g/mol], i_{corr} the corrosion current density [A/mm^2], Δt the duration of current application [s], z the anodic reaction valence [-], F Faraday's constant [96485 As/mol] and ρ the density of the metal [g/mm^3].

Considering Figure 2, the thickness of the free expanding corrosion products can be expressed as:

$$\Delta R_0 = R_2 - R_0 \quad (2)$$

The expansion of corrosion products is included in the model applying a fictitious thermal load to the corrosion layer as described in the following equation:

$$\Delta R_0 = (R_0 - R_1)\eta_{lin} \quad (3)$$

where η_{lin} is the linear expansion coefficient depending on the type of corrosion products formed. The linear expansion coefficient is described by a fictitious thermal expansion coefficient, α [K^{-1}], and a corresponding temperature increment, ΔT [K], see Equation (4).

$$\eta_{lin} = \alpha\, \Delta T \quad (4)$$

2.1 Penetration of corrosion products into the concrete matrix.

Figure 3 illustrates experimental results of accelerated corrosion tests observed by x-ray attenuation measurements in [14]. The figure clearly shows that corrosion products form in a non-uniform manner around the reinforcement and furthermore penetrate the surrounding concrete matrix and thereby delaying stress formation. Therefore, the penetration of corrosion products into the concrete matrix was included in the modeling scheme in [12,15] to reduce the effect of corrosion-induced expansion. The model was based on experimental data obtained from x-ray attenuation [12-14] and digital image correlation measurements [15] describing the penetration (time and depth) of corrosion products. From the experimental data a conceptual model (see Figure 4) to describe the penetration of corrosion products into the cementitious matrix was developed.

Based on the experimental results presented in [12-15], it is assumed that an initial corrosion accommodating region (CAR) around the reinforcement exists, denoted CAR_0, which delays stress formation while filling with solid corrosion products.

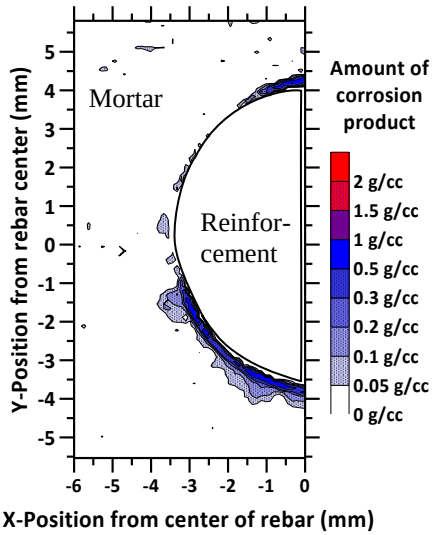

Figure 3: Contour plots highlighting penetration of corrosion products into mortar, from [14].

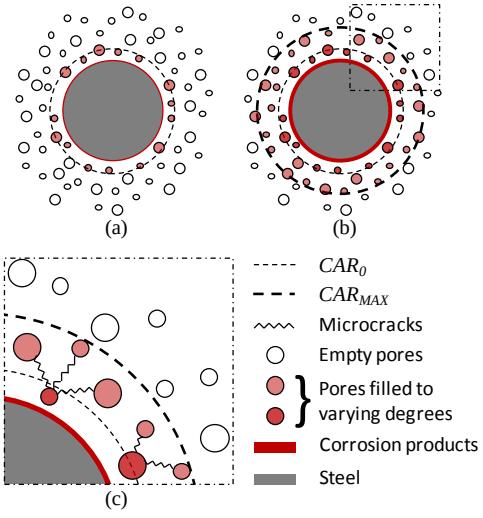

Figure 4: Conceptual schematic of idealized filling process of capillary porosity with corrosion products: (a) shows the initial *CAR*, CAR_0, (b) the subsequent increase in *CAR* size to a maximum, CAR_{MAX} and filling of additional pores due to (c) formation of micro-cracks between pores allowing movement of corrosion products, from [15].

Once this initial CAR_0 is filled with corrosion products, tensile stresses in the surrounding cementitious material will increase and potentially lead to the formation of micro-cracks. These micro-cracks allow solid corrosion products to penetrate additional pore spaces and further delay corrosion-induced stresses. At some point a maximum size of the CAR, denoted as CAR_{MAX}, is reached. No corrosion products can penetrate the matrix of the cementitious material beyond that point and all additionally formed corrosion products will introduce tensile stresses and potentially lead to the formation of a macro-crack.

Equations (5) and (6) express the observed characteristics of the CAR. κ describes the change in connectivity of capillary pores inside the CAR, t_{CAR_min} the time until CAR_0 is filled with corrosion products, t_{CAR_max} the time until CAR_{MAX} is filled with corrosion products, and t the time.

$$\kappa = \begin{cases} 0 & \text{if } t \le t_{CAR\_min} \\ t_c & \text{if } t_{CAR\_min} < t \le t_{CAR\_max} \\ 1 & \text{if } t > t_{CAR\_max} \end{cases} \quad (5)$$

where

$$t_c = \frac{t - t_{CAR\_min}}{t_{CAR\_max} - t_{CAR\_min}}$$

$$CAR = CAR_0 + (CAR_{MAX} - CAR_0)\kappa \quad (6)$$

Assuming the CAR consists of the capillary porosity of the cementitious material, φ, the CAR volume, V_{CAR}, may be determined as follows:

$$V_{CAR} = \varphi V_{CM} \quad (7)$$

where V_{CM} is the accessible volume of the cementitious matrix.

As mentioned before, a thermal analogy is used in the model to mimic the expansion of the corrosion products. The variation of the temperature increment in time is thereby calculated as shown in Equation (8), where ΔT_{CAR} is an adjusted equivalent temperature increment accounting for the impact of the CAR on corrosion-induced deformations and is applied in the FEM analysis instead of ΔT.

$$\Delta T_{CAR} = \lambda_{CAR} \Delta T \quad (8)$$

where λ_{CAR} describes the penetration of corrosion products into the accessible space of the cementitious matrix, V_{CAR}, and is described as follows:

$$\lambda_{CAR} = \begin{cases} \left(\frac{V_{cp}}{V_{CAR}}\right)^n & \text{if } V_{cp} < V_{CAR} \\ 1 & \text{if } V_{cp} \ge V_{CAR} \end{cases} \quad (9)$$

where n is an empirical parameter estimated to be 1.3 in [15]. Both the volume of the corrosion products, V_{cp}, and the volume of the CAR, V_{CAR}, are time dependent parameters, see e.g. Equations (1) and (5).

2.2 Creep

The effect of creep was implemented in the model in [15] according to Eurocode 2 [17] where the effective Young's modulus of the concrete matrix is adjusted at each time step according to Equation (10).

$$E_{c,eff} = \frac{E_c}{1 + \varphi(t,t_0)} \quad (10)$$

where $E_{c,eff}$ and E_c are the effective and secant Young's modulus [MPa], respectively, $\varphi(t,t_0)$ is the creep coefficient, which is a function of time, t the age of the concrete matrix [days] and t_0 the time at loading [days].

In the following a description of the modifications made to include the non-uniform formation of corrosion products is found.

2.3 Implementing non-uniform corrosion

Figure 5 illustrates the expansion mechanism of non-uniformly deposited corrosion products. The non-uniformity is implemented varying the corrosion current density around the circumference of the reinforcement and thereby generating different degrees of corrosion of the reinforcement - maintaining the same total corrosion current as in the uniform case. Mathematically the non-uniformity is modeled changing the corrosion current density from a scalar to a vector. This implies that Equation (1) is changed to Equation (11) in which the reinforcement radius reduction not only depends on time but also on the location.

The new vector describes the change in corrosion current density around the circumference of the reinforcement and thereby the shape of the corrosion layer. The shape is considered constant over time, which corresponds well to experimental observations made in [12,13,15].

$$\overrightarrow{X(t)} = \overrightarrow{R_0} - \overrightarrow{R_1} = \frac{M\,\overrightarrow{i_{corr}}\,\Delta t}{z\,F\,\rho} \qquad (11)$$

As Equation (11) is dependent on Equations (8) and (9), the partial penetration coefficient, λ_{CAR}, and the adjusted temperature increment, ΔT_{CAR}, are also dependent on the location.

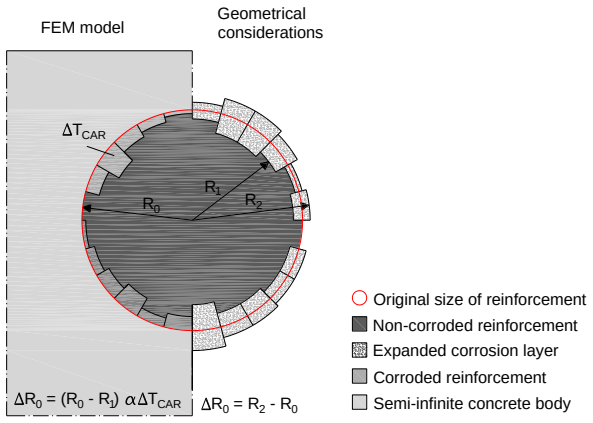

Figure 5: Load application (left) and basic geometrical considerations to model non-uniform formation of corrosion products (right) in the crack propagation model.

3 COMPARISON OF NUMERICAL AND EXPERIMENTAL DATA

The ability of the proposed model to simulate deformations and crack formation, induced by non-uniform deposition of corrosion products, is verified comparing, for a concrete body, numerical results with experimental observations presented in [15]. To compare numerical results with experimental results, the actual geometry of the test specimens was modeled.

In the experiment, a 23×100×100 mm^3 reinforced mortar specimen was subjected to corrosion impressing an electrical current of 100 μA/cm^2. To provide an electrical connection between working (reinforcement) and counter electrode (ruthenium/iridium electrode), the specimen was placed in tap water, which was maintained at a level of approximately 10 mm below the reinforcement, see Figure 6. One smooth 10 mm steel reinforcement bar was embedded in the center of the specimen and the water-to-cement ratio, w/c, of the mortar was 0.5.

Corrosion-induced deformations and crack formation were observed by means of digital image correlation (DIC) and the experiment was stopped when the first macro-crack was observed. For more information about the experimental approach the reader is referred to [15,18,19].

To simulate corrosion-induced deformations, the commercial FEM program DIANA 9.4.2 was used. 1766 elements (10,992 DOFs) were used to discretize the interface, concrete, reinforcement and corrosion layer domain in the model. Nonlinear solution of the problem was obtained using a standard Newton-Raphson method with a displacement controlled convergence criterion.

The input parameters for the numerical simulation are provided in Table 1. In the model the linear expansion coefficient is set to 0.7 assuming the formation of hematite (Fe_2O_3), which was confirmed by energy dispersive spectroscopy in [14]. The fictitious thermal expansion coefficient was set constant, i.e. 1, while the adjusted temperature increment, ΔT_{CAR}, accounted for the non-uniform deposition of corrosion products.

The experimental data was fitted adjusting the corrosion current density vector, $\overrightarrow{i_{corr}}$, in the FEM model. As starting point for the estimation of $\overrightarrow{i_{corr}}$, DIC measured deformations (after

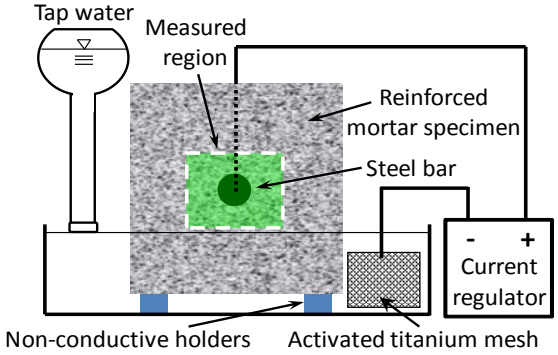

Figure 6: Experimental set up for DIC, from [15].

three days of accelerated corrosion) in the concrete/reinforcement interface were used. The resulting non-uniform $\overrightarrow{i_{corr}}$ around the circumference of the reinforcement (see Figure 5) provided a unique solution for all measurement times, see Figure 6.

Table 1: Input parameteres

Parameter	Value	Dimension
Length	23	mm
Width	100	mm
Height	100	mm
Concrete cover	45	mm
d_r	10	mm
RH	65	%
M_{Fe}	55.845	g/mol
z	2	-
ρ_{steel}	7.86	g/cm^3
F	96485	A·s/mol
$mean(i_{corr})$	0.0001	A/cm^2
CAR_0	0.14	mm
CAR_{MAX}	0.28	mm
η_{lin}	0.7	-
w/c	0.5	-
f_{cm}	45	MPa
E_c	32	GPa
μ_{conc}	0.2	-
f_{ct}	4.5	MPa
τ_{conc}	4.5	MPa
E_{steel}	210	GPa
μ_{steel}	0.3	-
E_{corr}	2	GPa
μ_{corr}	0.3	-

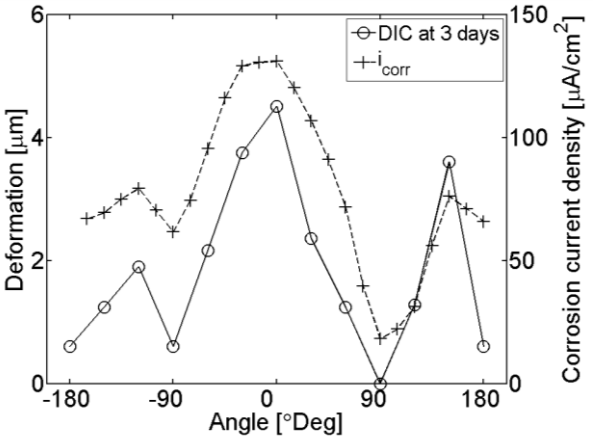

Figure 5: Illustration of measured deformations (dashed line) around the circumference of the reinforcement (solid line) at three days and the corresponding non-uniform corrosion current density.

Figure 6 illustrates a comparison of the modeled deformations at the concrete/reinforcement interface and experimentally measured deformations by DIC. In the figure, locations are described by polar coordinates where 90° marks the location of the predefined crack path. For the three different measurement times illustrated in the figure, the model predicts the corrosion-induced deformations very well. In general, the deviations at the different locations are less than 1 μm after six and nine days. When comparing the numerical and measured results for three days, higher deviations are found i.e. around 1 μm, which was accepted as the deviation decreased with time. For one point (150°) higher deviations between experimental and numerical results were found for three and six days. However, the deviation was not found after nine days and was therefore neglected. In the modeling approach it was assumed that the shape of the corrosion layer, i.e. non-uniform formation of corrosion products, is constant with time, which seems to be a fair assumption considering the comparison of the modeled and DIC measured deformations. The deviations that are seen for three days in general and at 150° for three and six days may be explained by small changes in the shape of the corrosion layer over time and due to microcracking, which is not included in the model.

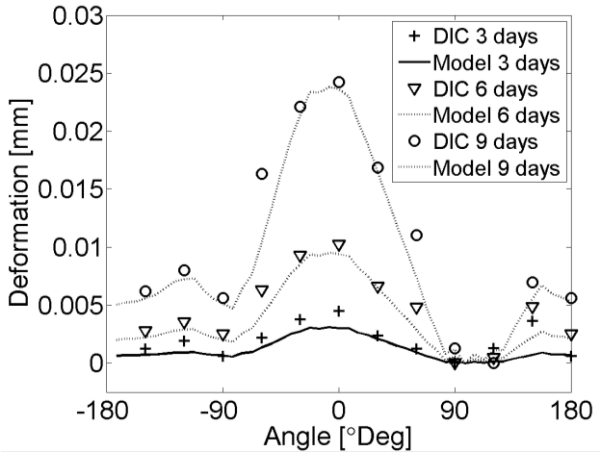

Figure 6: Modeled corrosion-induced deformations (lines) and corrosion-induced deformations measured by DIC (markers).

In Figure 7, the predicted corrosion-induced crack width is compared to the experimentally measured crack width. It should be noted that numerical predictions of the crack width are a result of the fitted corrosion-induced deformations at the concrete/reinforcement interface presented in Figure 6 and the material properties defined in Table 1. No additional fitting was performed.

To correspond to the location of the measured DIC crack width, the model predicted crack width was taken 1.4 mm from the reinforcement surface. In general, it is seen from the presented results that the modeled crack width corresponds well to the measured crack width. Both results, i.e. numerical and experimental, show a crack width of approximately 0 μm until six days after which the model predicted crack width rapidly increases. In contrast, the measured crack width starts to increase rapidly at approximately 7.5 days. Although, the numerical results do not capture the time-to crack initiation exactly, the model predicted crack width depicts the measured crack width well, as the slope of the two curves are approximately the same after 7.5 days. A reason for the deviation is most likely that micro-cracking is neglected in the present model. In the experiment two micro-cracks were observed and the formation of these micro-cracks has most likely postponed the initiation of the third crack (macro-crack).

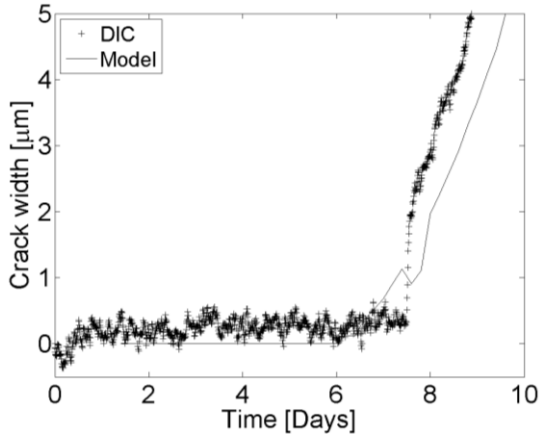

Figure 7: Modeled corrosion-induced crack width (line) and crack width measured by DIC (markers) at 1.4 mm from the reinforcement surface.

Additional uncertainty in the model is the Young's modulus of corrosion products. In the present model a value of 2.0 GPa was used as proposed in [15]. Furthermore, it should be noted that studies in [15] showed a weak dependence of corrosion-induced deformations on the Young's modulus of corrosion products.

4 INFLUENCE OF MODELING NON-UNIFORM CORROSION ON SURFACE CRACKING

To demonstrate the impact of non-uniform deposition of corrosion products on the time-to crack initiation and crack propagation, a numerical example is given. In the example, the crack width at the concrete surface (CWCS) is compared for four different scenarios, which are illustrated in Figure 8 and defined in Table 2. The different scenarios represent situations in which the main part of corrosion products accumulate in one area and are subsequently compared to a scenario assuming uniform deposition of corrosion products. For each scenario the model is set to simulate 40 days of impressed current. Parameters used for the simulations are provided in Table 1. The width and height of the concrete body were changed to 210 mm and 155 mm, respectively. The values for the width and height of the concrete (assuming semi-infinite behavior) were based on a study presented in [10].

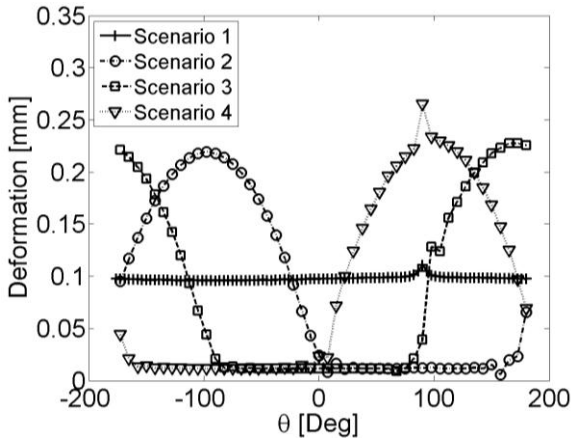

Figure 8: Illustration studied scenarios. θ describes the location around the circumference of the reinforcement in polar coordinates. Please note: the figure illustrates corrosion-induced deformations at 40 days.

Locations around the circumference of the reinforcement are described in polar coordinates in Figure 9 along with a clock reference (numbers inside circle) and placement of the predefined corrosion-induced crack path.

Table 2: Scenarios investigated.

Scenario	Characteristic
1	Uniform shape
2	Vertex at 6 o'clock
3	Vertex at 9 o'clock
4	Vertex at 12 o'clock

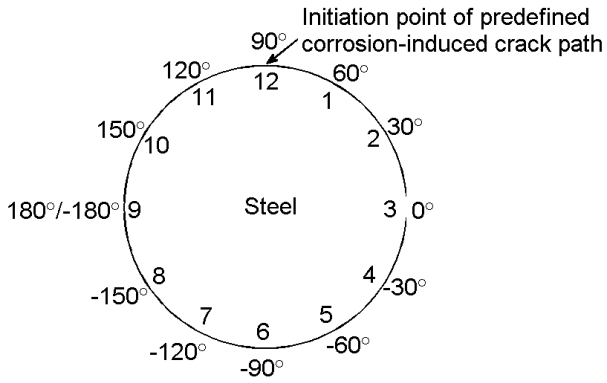

Figure 9: Placement of angles (numbers outside circle) in the circumference of the reinforcement together with a clock reference (numbers inside circle). The crack initiates at 12 o'clock (90°).

5 RESULTS

In Figure 10, the crack width at the concrete surface is illustrated as a function of time for the four different scenarios.

In general, a considerable difference is seen regarding both time-to cover cracking and crack width for the investigated scenarios. For scenario 2, the crack is initiated after approximately 14 days, which is six days later than for scenario 3 and eight days later than for scenario 4. It should be noted that under natural conditions the difference in time-to cover cracking could in fact be years instead of days as the corrosion current density under natural conditions is considerably smaller. Also, the crack width at the concrete surface for scenario 4 is 21% bigger than for scenario 3 and 63% bigger than for scenario 2, see Table 3. Comparing scenario 1 (uniform formation of corrosion products) with the three other scenarios, it is seen that the assumption of uniform corrosion can lead to considerable underestimations of the time-to corrosion-induced cover cracking. Both the comparison of the time-to corrosion-induced cover cracking and crack widths illustrate the importance of understanding and modeling non-uniform deposition of corrosion products. A realistic method to implement this mechanism could be a probabilistic modeling approach. The presented results may thereby be seen as a first step illustrating extreme scenarios and providing impertinent information on the uncertainty of time-to corrosion-induced cracking.

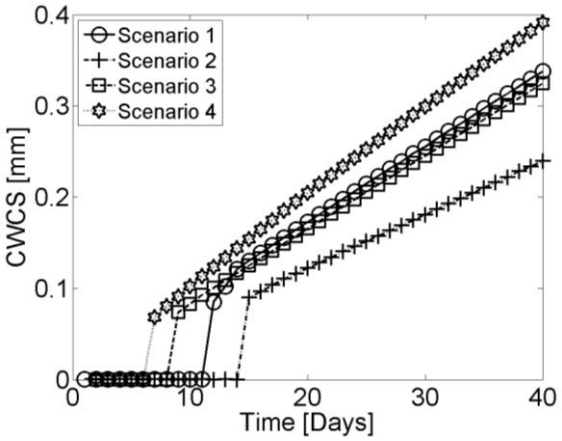

Figure 10: Crack width at concrete surface, CWCS, as a function of time.

Table 3: Time-to cover cracking and crack width at the concrete surface after 40 days.

Scenario	Initiation of CWCS [Days]	Final CWCS [mm]
1	11	0.3377
2	14	0.2394
3	8	0.3245
4	6	0.3912

6 SUMMARY AND CONCLUSIONS

In the present paper, the non-uniform deposition behavior of corrosion products is included in the modeling scheme of an existing deterministic finite element fracture model. The non-uniformity was implemented varying the corrosion current density along the circumference of the reinforcement. In the model, penetration of corrosion product was included but

micro-cracking and the influence of cracks on transport properties of the concrete was not considered.

To verify the model, digital image correlation measurements of deformations and crack widths were compared to simulated results. Comparisons between experimental observations and numerical results showed that the model simulates both deformations and crack width in accordance with measured data.

To investigate the influence of non-uniform deposition of corrosion products, a numerical example was given. In the example four different scenarios (accumulation of corrosion products at different locations along the circumference of the reinforcement) were studied. Comparison between the studied scenarios, showed considerable differences in the time-to cover cracking and the crack width at the surface. For scenario 4 (accumulation of corrosion products at crack initiation point) the shortest time-to cover cracking and largest final crack width was found. Based on the results presented in this study, it is recommended that future investigations and modeling of corrosion-induced cracking should focus on non-uniform deposition of corrosion products.

7 ACKNOWLEDGMENTS

The authors gratefully acknowledge the financial support of the Danish Expert Centre for Infrastructure Constructions. Further, the authors would like to thank Bradley J. Pease for contributing with experimental data.

REFERENCES

[1] Rendell, F., Jauberthie, R. and Grantham, M., 2002. *Deteriorated Concrete - Inspection and physicochemical analysis*. Thomas Telford.

[2] Alonso, C., Andrade, C., Rodriguez, J. and Diez, J., 1998. Factors controlling cracking of concrete affected by reinforcement corrosion. *Materials and Structures.* **31**:435-441.

[3] Andrade, C., Alonso, C. and Molina, F.J., 1993. Cover cracking as a function of bar corrosion: Part 1-Experimental test. *Materials and Structures,* **26**:453-464.

[4] Liu, Y. and Weyers, R.E., 1998. Modeling the Time-to-Corrosion Cracking in Chloride Contaminated Reinforced Concrete Structures. *Corrosion,* **95**:675-681.

[5] Chernin, L., Val, D.V. and Volokh, K.Y., 2010. Analytical modelling of concrete cover cracking caused by corrosion of reinforcement. *Materials and Structures,* **43**:543-556.

[6] Molina, F., Alonso, C. & Andrade, C., 1993. Cover cracking as a function of rebar corrosion: Part 2-Numerical model. *Materials and Structures,* **26**:532-548.

[7] Noghabai, K., 1999. FE-Modelling of cover splitting due to corrosion by use of inner softening band. *Material and Structures*, **32**:486-491.

[8] Biondini, F. and Vergani, M., 2012. Damage modeling and nonlinear analysis of concrete bridges under corrosion. In F. Biondini and D. M. Frangopol (eds), *Bridge Maintenance, Safety, Management, Resilience and Sustainability; Proc. of the 6th Inter. Conf. on Bridge Maintenance, Safety and Management (IABMAS 2012),* July 8-12, 2012, Stresa, Italy: pp.949-957.

[9] Isgor, O.B. and Razaqpur, A.G., 2006. Modelling steel corrosion in concrete structures. *Materials and Structures,* **39**:291-302.

[10] Michel, A., Solgaard, A.O.S., Geiker, M., Stang, H. and Olesen, J.F.,2010. Modeling Formation of Cracks in Concrete Cover due to Reinforcement Corrosion. *Proc. of 7th Inter. Conf. on Fract. Mech. of Conc. & Conc. Struct. (FraMCoS-7),* May 23-28, 2010, Jeju, South Korea: pp.944-951.

[11] Solgaard, A.O.S., Michel, A. and Stang, H., Submitted. Concrete Cover Cracking due to uniform reinforcement corrosion. *Materials and Structures.*

[12] Michel, A., Pease, B.J., Peterová, A. and Geiker, M., 2012. Experimental determination of the penetration depth of corrosion products and time to corrosion-induced cracking in reinforced cement based materials. *Proc. of Inter. Cong. On Durability of Conc. (ICDC 2012),* July 17-21, 2012, Trondheim, Norway.

[13] Pease, B.J., Michel, A. & Stang, H., 2012. Quantifying movements of corrosion products in reinforced concrete using x-ray attenuation measurements. *Proc. of the 2nd Inter. Conf. on Microstructure Related Durability of Cementitious Composites (MicroDurability),* April 11-13, 2012, Amsterdam, The Netherlands.

[14] Michel, A., Pease, B.J., Geiker, M., Stang, H. and Olesen, J.F., 2011. Monitoring reinforcement corrosion and corrosion-induced cracking using non-destructive x-ray attenuation measurements. *Cement and Concrete Research,* **41**:1085-1094.

[15] Pease, B.J., Michel, A., Thybo, A.E.A. and Stang, H., 2012. Estimation of elastic modulus of reinforcement corrosion products using inverse analysis of digital image correlation measurements for input in corrosion-induced cracking model. In F. Biondini and D. M. Frangopol (eds), *Bridge Maintenance, Safety, Management, Resilience and Sustainability; Proc. of the 6th Inter. Conf. on Bridge Maintenance, Safety and Management (IABMAS 2012),* July 8-12, 2012, Stresa, Italy: pp.3643-3650.

[16] Val, D.V., Chernin, L. and Stewart, M. G., 2009. Experimental and numerical investigation of corrosion-induced cover cracking in reinforced concrete structures. *J. of Structural Engineering,* **135**: 376-385.

[17] Eurocode 2, 2003. Design of Concrete Structures. European Committee for Standardization (CEN).

[18] Pease B, Geiker M, Stang H. and Weiss J., 2006, Photogrammetric assessment of flexure induced cracking of reinforced concrete beams under service loads. In J. Marchand, B. Bissonnette, R. Gagné, M. Jolin and F. Paradis. Proc. *2nd Inter. RILEM Symposium Advances in Conc. through Science and Engineering*, Québec, Canada.

[19] Pereira, E., Fischer, G. and Barros, J., 2011, Image-based detection and analysis of crack propagation in cementitious composites. In: C. Leung (eds), *Proc. of Inte. Conf. on Advances in Construction Materials through Science and Engineering*, Hong Kong, China.